New Fast and Accurate Line Parameter Calculation of General Multiconductor Transmission Lines in Multilayered Media

Frank Olyslager, *Student Member, IEEE*, Niels Faché, and Daniël De Zutter

Abstract—**This paper presents a considerably enhanced method to calculate C, L, and R of a multiconductor bus in a multilayered medium. Different board technologies, conductors of complicated shape, and conductors embedded in different layers can be handled without loss of accuracy or substantial increase in CPU time compared with existing simulation techniques. Correct determination of skin effect losses is shown to depend critically on surface charge modeling. Surface charge discontinuities are explicitly taken into account, which results in reduced computation time. A further reduction of computation time is obtained by a new treatment of the calculation of the Green's function.**

I. Introduction

In recent years much theoretical effort has been invested in modeling multiconductor transmission lines in multilayered media in the quasi-TEM limit [1]–[3] as well as in the full-wave regime [4]–[7]. Starting from the findings presented in previous work and adding a number of innovations, it was our purpose to develop a very fast, and at the same time accurate, software package for the line parameters of a general electrical bus configuration in the quasi-TEM limit.

Owing to the importance of a controlled impedance for high-speed signal transport in computers and telecommunication, flexible design of multiconductor buses becomes increasingly important. The theory presented in this paper and its implementation on modern workstations allow for real-time use in circuit simulators which predict the signal behavior (crosstalk, reflection, pulse propagation, etc.) of electrical bus configurations. Our approach explicitly includes a detailed modeling of conductors with curved sides or of circular cross section. This allows us to handle new technologies such as discrete wiring boards and to study the influence of the rounding of edges or of underetching in detail.

Manuscript received July 31, 1990; revised January 22, 1991. This work was supported by the National Fund for Scientific Research of Belgium (NFWO).

The authors are with the Laboratory of Electromagnetism and Acoustics, University of Ghent, Sint-Pietersnieuwstraat 41, 9000 Ghent, Belgium.

IEEE Log Number 9144285.

We use an integral equation for the surface charges on the conductors which is solved by the point-matching or collocation technique. The kernel of the integral equation is an appropriate Green's function of the layered medium. This Green's function is calculated in the spectral domain with a new technique, first discussed in [8]. This technique allows us to interchange the inverse spatial Fourier transform with the integration over the conductor surfaces. Interchanging the integrations has two benefits. In many cases the integration over the conductor surface can be done analytically or results in integrations which can be performed accurately with special quadrature formulas. A second advantage is that the integration over the conductor surface can be done once for almost all the point-matching points, which results in a fast algorithm.

The basis functions used in the expansion of the surface charge density are very general. In Sections IV and VI the use of piecewise-linear basis functions is explained. Our algorithm is also applicable to representations that are piecewise-constant, piecewise-parabolic, piecewise-cubic, etc., as will be demonstrated in the examples. In all cases the special behavior of the surface charge density at edges and layer interfaces is taken into account as predicted by Meixner [9].

We also extended our algorithm to include small losses caused by the skin effect in the conductors and ground planes. We adopted and modified the method of [3] for the Green's function of the layered medium. This allows us to handle stripline configurations without having to approximate the second ground plane by a finite conductor and to handle multilayered permeable media. The necessity to extend the surface charge modeling beyond a piecewise-constant representation in order to obtain accurate results for the resistance matrix is demonstrated in Section VII.

The examples given in Section VII demonstrate the accuracy and generality of our method.

II. Geometry

The structure under consideration is a multilayered one (Fig. 1). Each of the L layers is homogeneous and isotropic and has an arbitrary relative permittivity $\epsilon_{r,i}$, relative

0018-9480/91/0600-0901$01.00 ©1991 IEEE

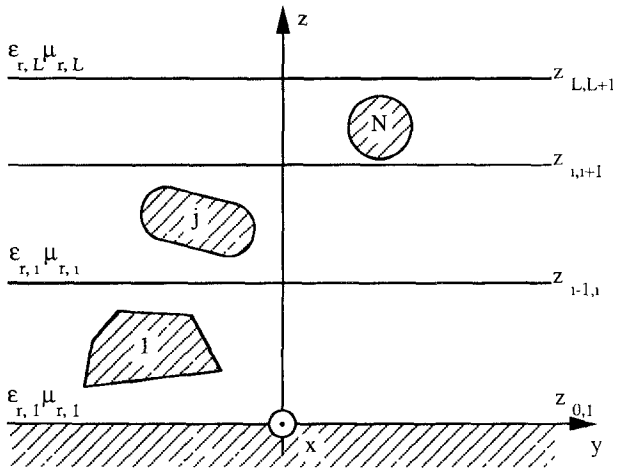

Fig. 1. Geometry of a general multiconductor electrical bus in a multilayered medium.

permeability $\mu_{r,i}$, and thickness d_i. At the top and bottom of the structure we have either a semi-infinite layer or a perfectly conducting metal plane. This means that we distinguish three types of geometries: open (no metal plane), half-open (one metal plane), and closed (two metal planes). There are N conductors, which are bounded by a combination of straight and curved sides. We restrict ourselves to curved sides which are parts of a circle or of an ellipse. More general curved sides, however, can easily be included. These conductors may be located in more than one layer at the same time. We choose a right-hand coordinate system with the x axis parallel to the conductors, the y axis parallel to the layers in the cross section, and the z axis perpendicular to the layers. The quantity $z_{i-1,i}$ is the z coordinate of the layer interface between layer $i-1$ and layer i. The proposed solution is valid for very good conductors with small losses due to the skin effect.

III. Outline of the Solution

In the first place we search the capacitance matrix, $\boldsymbol{C}$, of the structure under consideration. To find $\boldsymbol{C}$ we make use of the classical integral equation for the surface charge density. As a matter of completeness and in order to introduce certain notation, we will give a short derivation of this integral equation.

Element j,k of $\boldsymbol{C}$ follows from

$$\boldsymbol{C}_{j,k} = \oint_{c_j} \rho_j^k(\boldsymbol{r})\, dc, \qquad j,k = 1,\cdots,N \tag{1}$$

where c_j is the boundary of conductor j and $\rho_j^k(\boldsymbol{r})$ is the surface charge density on conductor j when conductor k is on 1 V and all the other conductors are 0 V. The potential $\phi^k(\boldsymbol{r})$ generated by $\rho_j^k(\boldsymbol{r})$ in the layered medium is given by

$$\phi^k(\boldsymbol{r}) = \sum_{j=1}^{N} \oint_{c_j} \rho_j^k(\boldsymbol{r}')G(\boldsymbol{r}|\boldsymbol{r}')\, dc', \qquad k = 1,\cdots,N \tag{2}$$

where $G(\boldsymbol{r}|\boldsymbol{r}')$ is the Green's function of the layered medium. We find the required integral equation for the unknown surface charge densities $\rho_j^k(\boldsymbol{r})$ by requiring that $\phi^k(\boldsymbol{r})$ be 1 V on conductor k and 0 V on all other conductors; hence

$$\lim_{\boldsymbol{r}\to\boldsymbol{r}_i} \sum_{j=1}^{N} \oint_{c_j} \rho_j^k(\boldsymbol{r}')G(\boldsymbol{r}|\boldsymbol{r}')\, dc' = \delta_{i,k}, \qquad i,k = 1,\cdots,N \tag{3}$$

where $\delta_{i,k}$ is the Kronecker delta. This integral equation is solved with the method of moments combined with collocation or point matching. The Green's function is found in the spatial Fourier domain with respect to the y direction. The spatial Green's function, $G(\boldsymbol{r}|\boldsymbol{r}')$, follows from an inverse Fourier transformation of the spectral Green's function $G(k_y, z|z')$:

$$G(\boldsymbol{r}|\boldsymbol{r}') = \frac{1}{\pi}\int_0^{+\infty} G(k_y, z|z')\cos\left[k_y(y-y')\right] dk_y. \tag{4}$$

We introduce an asymptotic Green's function, $G^{\text{as}}(k_y, z|z')$, which is equal to the full Green's function, $G(k_y, z|z')$, for high k_y values. Now we define a finite Green's function, $G^{\text{fin}}(k_y, z|z')$, as

$$G^{\text{fin}}(k_y, z|z') = \begin{cases} G(k_y, z|z'), & 0 < k_y < k_c \\ G(k_y, z|z') - G^{\text{as}}(k_y, z|z'), & k_c < k_y < k_e \\ 0, & k_e < k_y < +\infty \end{cases}. \tag{5}$$

The constants k_c and k_e are suitably chosen constants which must be chosen such that a good balance is reached between numerical accuracy and CPU time requirements. At k_e the difference between $G(k_y, z|z')$ and $G^{\text{as}}(k_y, z|z')$ becomes negligible.

We can rewrite (3) using (5):

$$\begin{aligned} &\sum_{j=1}^{N} \frac{1}{\pi}\int_0^{k_e} \oint_{c_j} \rho_j^k(\boldsymbol{r}')G^{\text{fin}}(k_y, z_i|z') \\ &\qquad \cdot\cos\left[k_y(y_i - y')\right] dc'\, dk_y \\ &+ \sum_{j=1}^{N} \lim_{\boldsymbol{r}\to\boldsymbol{r}_i} \frac{1}{\pi} \oint_{c_j} \rho_j^k(\boldsymbol{r}') \int_{k_c}^{+\infty} G^{\text{as}}(k_y, z|z') \\ &\qquad \cdot\cos\left[k_y(y-y')\right] dk_y\, dc' = \delta_{i,k}, \\ &\qquad\qquad i,k = 1,\cdots,N. \end{aligned} \tag{6}$$

For the asymptotic integration we cannot interchange the integration and the limiting operation owing to self-patch contributions. Indeed, interchanging the two operations would lead to divergent integrals.

The inductance matrix, $\boldsymbol{L}$, is found as the inverse matrix of the capacitance matrix of the same geometry but with the permittivity of each layer replaced by the inverse of the permeability.

The resistance matrix, $\boldsymbol{R}$, arising from losses in the conductors and ground planes is found with the method

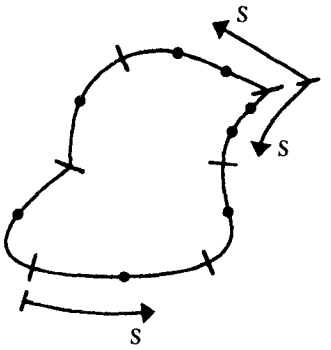

Fig. 2. Conductor surface divided into segments and point-matching points with s the arc length for each segment measured from one end point of the segment.

described in [3]. Our method used for the losses in the ground planes is different and more general from the applied method in [3]. Our method allows layers of differing permeability. In contrast to [3], no distinction is made between an upper and a lower ground plane because we use the Green's function of the layered medium. We need to calculate the integral over the ground plane of the square of the surface current, J_x. This surface current, J_x, is found as the surface charge density, ρ, in the equivalent electrostatic problem used to calculate $\boldsymbol{L}$. The charge density itself is found from the z derivative of the potential at the ground plane(s). For the integration over the ground plane(s) a Gaussian quadrature integration is used.

IV. Discretization of the Integral Equation

We divide the surface of each conductor into a number of segments (Fig. 2). Let s be the distance from one end point of the segment to a point on the segment. If one of the end points of the segment is a corner of the conductor, we choose $s=0$ at this particular end point. We represent the surface charge density, $\rho(s)$, along the segment as

$$\rho(s) = s^{\mu}(A_0 + A_1 s), \qquad \mu \geqslant -0.5. \tag{7}$$

A_0 and A_1 are the unknowns for the considered segment, and μ follows from Meixner's edge conditions [9]; e.g., $\mu = -0.5$ at the end points of infinitely thin conductors.

At the junction of two segments we impose the continuity of the surface charge density. This already places a first restriction on the unknowns. We have chosen this representation and not a representation with triangular basis functions as in [1] because each term can be handled in the same way and because this representation can easily be extended to more general representations. By simply adding a term we go from a piecewise-linear to a piecewise-parabolic representation, as will be illustrated in Section VII.

The point-matching points are chosen in the middle of each segment. Along corner segments we take two point-matching points to get a stable solution. Because of this small oversampling we obtain a system of equations with slightly more equations than unknowns. This system is solved in the least square sense.

V. The Spectral Green's Function

The spectral Green's function of the layered medium is the solution of

$$\frac{d^2}{dz^2}G(k_y, z|z') - k_y^2 G(k_y, z|z') = \delta(z - z'). \tag{8}$$

The layer in which z' is located is called the excitation layer, e. We introduce new relative z coordinates with respect to the bottom and top of layer e: $w_e = z' - z_{e-1,e}$ and $v_e = z_{e,e+1} - z'$. A column vector, $\boldsymbol{c}(z)$, is defined as

$$\boldsymbol{c}(z) = \begin{pmatrix} G(k_y, z|z') \\ -\dfrac{1}{k_y Z}\dfrac{d}{dz}G(k_y, z|z') \end{pmatrix}, \qquad Z = -\frac{1}{\epsilon_r \epsilon_0 k_y}. \tag{9}$$

The vector $\boldsymbol{c}(z)$ is continuous at layer interfaces, where we use the shorthand notation $\boldsymbol{c}(z = z_{i-1,i}) = \boldsymbol{c}_{i-1,i}$. It is determined using the methods described in [1] and [6] with, however, an important modification (first discussed in [8]) in order to have explicit dependence on the excitation position. When we "role up" the layers above and under the excitation we get the following representation at the top and bottom of the excitation layer:

$$\boldsymbol{c}_{e-1,e} = \prod_{i=1}^{e-1} \boldsymbol{N}_i^u \boldsymbol{K}^u \exp(k_y d_i) D_1$$

and

$$\boldsymbol{c}_{e,e+1} = \prod_{i=L}^{e+1} \boldsymbol{N}_i^d \boldsymbol{K}^d \exp(k_y d_i) D_L \tag{10}$$

with

$$\boldsymbol{N}_i^u = \frac{1}{2}\begin{pmatrix} 1+\exp(-2k_y d_i) & -Z_i[1-\exp(-2k_y d_i)] \\ -1/Z_i[1-\exp(-2k_y d_i)] & 1+\exp(-2k_y d_i) \end{pmatrix}$$

$$\boldsymbol{N}_i^d = \frac{1}{2}\begin{pmatrix} 1+\exp(-2k_y d_i) & Z_i[1-\exp(-2k_y d_i)] \\ 1/Z_i[1-\exp(-2k_y d_i)] & 1+\exp(-2k_y d_i) \end{pmatrix} \tag{11}$$

and

$$\boldsymbol{K}^u = \begin{pmatrix} s \\ -1/Z_1 \end{pmatrix} \quad \text{and} \quad \boldsymbol{K}^d = \begin{pmatrix} -s \\ -1/Z_L \end{pmatrix}. \tag{12}$$

In the presence of a ground (top) plane, $s = 0$ in $\boldsymbol{K}^u$ ($\boldsymbol{K}^d$) and Z_1 (Z_L) is the Z value belonging to the layer immediately above (below) the ground (top) plane. If the bottom (top) layer of the medium is semi-infinite, then $s = 1$ and Z_1 (Z_L) is the Z value belonging to this layer. D_1 and D_L are unknowns to be found by the procedure explained below.

Now we replace D_1 and D_L by new unknowns R_1^o and R_L^o:

$$R_L^o = \prod_{i=L}^{e} \exp(k_y d_i) D_L \quad \text{and} \quad R_1^o = \prod_{i=1}^{e-1} \exp(k_y d_i) D_1. \tag{13}$$

For further use we introduce two new column vectors, $\boldsymbol{c}_{e-1,e}^d$ and $\boldsymbol{c}_{e-1,e}^u$:

$$\boldsymbol{c}_{e-1,e}^d = \prod_{i=L}^{e} \boldsymbol{N}_i^d \boldsymbol{K}^d R_L^o \quad \text{and} \quad \boldsymbol{c}_{e-1,e}^u = \prod_{i=1}^{e-1} \boldsymbol{N}_i^u \boldsymbol{K}^u R_1^o. \tag{14}$$

We also introduce two matrix functions, $\boldsymbol{M}^d(\Delta z)$ and $\boldsymbol{M}^u(\Delta z)$, in the variable Δz:

$$\boldsymbol{M}^d(\Delta z) = \begin{pmatrix} \operatorname{ch}(k_y \Delta z) & Z_e \operatorname{sh}(k_y \Delta z) \\ 1/Z_e \operatorname{sh}(k_y \Delta z) & \operatorname{ch}(k_y \Delta z) \end{pmatrix}$$

$$\boldsymbol{M}^u(\Delta z) = \begin{pmatrix} \operatorname{ch}(k_y \Delta z) & -Z_e \operatorname{sh}(k_y \Delta z) \\ -1/Z_e \operatorname{sh}(k_y \Delta z) & \operatorname{ch}(k_y \Delta z) \end{pmatrix}. \tag{15}$$

The variable Δz will take values v_e and w_e in the sequel. Starting from (8), (9), (10), (13), (14), and (15), the following relations are found to hold at z':

$$\boldsymbol{M}^d(v_e)\boldsymbol{c}_{e,e+1} - \boldsymbol{M}^u(w_e)\boldsymbol{c}_{e-1,e} = \begin{pmatrix} 0 \\ 1 \end{pmatrix} \tag{16}$$

and

$$\boldsymbol{M}^u(w_e)\boldsymbol{c}_{e-1,e}^d - \boldsymbol{M}^u(w_e)\boldsymbol{c}_{e-1,e}^u = \begin{pmatrix} 0 \\ 1 \end{pmatrix}. \tag{17}$$

Finally (17) yields, after left multiplying with $[\boldsymbol{M}^u(w_e)]^{-1}$,

$$\boldsymbol{c}_{e-1,e}^d - \boldsymbol{c}_{e-1,e}^u = \begin{pmatrix} Z_e \operatorname{sh}(k_y w_e) \\ \operatorname{ch}(k_y w_e) \end{pmatrix} \tag{18}$$

We have replaced the original excitation, $\begin{pmatrix} 0 \\ 1 \end{pmatrix}$, at z' by a new excitation, $\boldsymbol{b} = \begin{pmatrix} Z_e \operatorname{sh}(k_y w_e) \\ \operatorname{ch}(k_y w_e) \end{pmatrix}$, at the bottom of the excitation layer. The two linear equations in (18) are in the unknowns R_1^o and R_L^o. Let the solution for $\boldsymbol{b} = \begin{pmatrix} 1 \\ 0 \end{pmatrix}$ be (v_1^o, v_L^o) and for $\boldsymbol{b} = \begin{pmatrix} 0 \\ 1 \end{pmatrix}$ be (i_1^o, i_L^o). By superposition we get, for R_1^o and R_L^o,

$$R_1^o = Z_e \operatorname{sh}(k_y w_e) v_1^o + \operatorname{ch}(k_y w_e) i_1^o$$

$$R_L^o = Z_e \operatorname{sh}(k_y w_e) v_L^o + \operatorname{ch}(k_y w_e) i_L^o. \tag{19}$$

Suppose we want to know $G(k_y, z|z')$ at an observation level $z > z'$ in layer o. We define relative coordinates $w_o = z - z_{o-1,o}$ and $v_o = z_{o,o+1} - z$ where $z_{o-1,o}$ and $z_{o,o+1}$ are the bottom and top coordinate of the observation layer o. Now its easy to find the Green's function [1], [6]:

$$\begin{aligned} G(k_y, z|z') = \{ & A_{e,o} \exp[k_y(v_o + w_e - d_e)] \\ & + B_{e,o} \exp[k_y(v_o - w_e - d_e)] \\ & + C_{e,o} \exp[k_y(-v_o + w_e - d_e)] \\ & + D_{e,o} \exp[k_y(-v_o - w_e - d_e)] \} \\ & \cdot \prod_{i=o}^{e+1} \exp(-k_y d_i). \end{aligned} \tag{20}$$

The coefficients $A_{e,o}$, $B_{e,o}$, $C_{e,o}$, and $D_{e,o}$ depend only on the positions of the excitation and observation layers and not on the exact positions of the excitation and observation levels themselves. These coefficients have to be calculated only once for each observation–excitation layer couple. We have found the explicit analytical dependence on the excitation level z' which allows us to have an explicit argument in the integration over the excitation segment. In some cases we will be able to perform this integration analytically. The form (20) and the derivation leading to it can only be used for observation levels above the excitation in order to have exponentially decaying terms in all numerical calculations. For observation points under the excitation we transform the excitation to the top of the excitation layer. However, the result can also be found immediately from (20) by making use of reciprocity.

For the asymptotic Green's function, $G^{\text{as}}(k_y, z|z')$, only four waves, going from excitation to observation position, are taken into account. We obtain the following expression for $G^{\text{as}}(k_y, z|z')$ when $z > z'$:

$$\begin{aligned} G^{\text{as}}(k_y, z|z') = & \frac{Z_e}{2} \{ \exp[k_y(v_o + w_e - d_e)] \\ & + K_{e-1,e}^d \exp[k_y(v_o - w_e - d_e)] \\ & + K_{o,o+1}^u \exp[k_y(-v_o + w_e - d_e)] \\ & + K_{o,o+1}^u K_{e,e+1}^u \exp[k_y(-v_o - w_e - d_e)] \} \\ & \cdot \prod_{i=o}^{e+1} T_{i-1,i}^u \exp(-k_y d_i). \end{aligned} \tag{21}$$

The first term corresponds to a wave which travels directly from excitation to observation. The second term is a wave which is reflected from the bottom of the excitation layer and then travels to the observation. The third term is a wave which is reflected from the top of the observation layer and the last term represents a wave which is reflected from both the top of the observation layer and the bottom of the excitation layer. The reflection and transmission coefficients K and T are given by

$$K_{i,i+1}^u = \frac{\epsilon_i - \epsilon_{i+1}}{\epsilon_i + \epsilon_{i+1}} \qquad K_{i-1,i}^d = \frac{\epsilon_i - \epsilon_{i-1}}{\epsilon_i + \epsilon_{i+1}}$$

$$T_{i-1,i}^u = \frac{2\epsilon_{i-1}}{\epsilon_{i-1} + \epsilon_i}. \tag{22}$$

TABLE I
CAPACITANCE AND RESISTANCE, USING DIFFERENT NUMERICAL APPROACHES, FOR A WIRE WITH DIAMETER $d = 1$ LOCATED IN A SEMI-INFINITE DIELECTRIC WITH $\epsilon_r = 4$ AT A HEIGHT $H = 2$ ABOVE A GROUND PLANE

	C (F/m)	R/R_s (1/m)
Parabolic representation with eight segments	1.07867 e-10	0.32875
Linear representation with eight segments	1.07870 e-10	0.32882
Linear representation with 24 segments	1.07847 e-10	0.32875
Harrington and Wei [3]	1.073 e-10	0.3299
Analytical formula [3]	1.07844 e-10	0.32875

TABLE II
CAPACITANCE AND RESISTANCE FOR THE WIRE USED IN TABLE I FOR DIFFERENT VALUES OF H

H		Piecewise Parabolic 8 Divisions	Piecewise Linear 24 Divisions	Analytical Formula [3]
3	C (F/m)	8.98222 e-11	8.98075 e-11	8.98063 e-11
3	R (1/m)	0.32282	0.32283	0.32283
4	C (F/m)	8.03832 e-11	8.03755 e-11	8.03746 e-11
4	R (1/m)	0.32083	0.32083	0.32083
5	C (F/m)	7.43519 e-11	7.43454 e-11	7.43446 e-11
5	R (1/m)	0.31991	0.31991	0.31991

VI. THE INTEGRATIONS

A. Finite Spectral Integral Contribution

First we will pay attention to the first term in (6). The Green's function (20) and the charge density representation (7) are substituted in (6). The integration over k_y is done numerically by means of a Gauss quadrature integration. For an integration over the excitation segment we make a distinction between linear and curved segments. For linear segments the first term of (6) yields integrals of the following form:

$$I_\nu = \int_{s_0}^{s_1} s^\nu \exp(as)\cos(b - sc)\, ds \tag{23}$$

where a, b, and c are constants. When ν is an integer, I_ν is calculated analytically; otherwise a Gauss–Jacobi or Gauss quadrature integration is used, depending on whether s_0 is zero or not. The case where ν is not an integer occurs only for segments at the corners of the conductors.

For circular and elliptic segments the first term of (6) yields integrals of the following form:

$$I_\nu = \int_{\phi_0+\phi_c}^{\phi_1+\phi_c} (\phi - \phi_c)^\nu \exp[a\sin(\phi)] \cdot \left\{ \begin{matrix} \cos[b - c\cos(\phi)] \\ \sin[b - c\cos(\phi)] \end{matrix} \right\} \cdot \sqrt{a^2\cos^2(\phi) + c^2\sin^2(\phi)}\, d\phi \tag{24}$$

where a, b, c, and ϕ_c are constants. When $|a| = |c|$ we have circular segments; when $|a| \neq |c|$ we have elliptic segments. The integrations are performed using a Gauss–Jacobi quadrature if $\phi_0 = 0$ and a simple Gauss quadrature if $\phi_0 \neq 0$. The same technique can be applied to more general segments with other parameter representations. The quantities s_0 in (23) and ϕ_0 in (24) are different from zero when the observation point and the points of the excitation segment have the same z coordinate. This is because we have to use another Green's function for the part of the excitation segment above and the part under the observation point. The integration over the excitation segment needs to be performed only once for all observation points, except when there are observation points at the same level as the excitation segment.

B. Infinite Spectral Integral Contribution

Now we will take a closer look at the second term in (6). We again insert the asymptotic Green's function (21) and the charge density representation (7) in this second term. For linear segments we get integrals of the following form:

$$I_\nu = \int_{k_c}^{+\infty} \frac{\exp(-k_y d)}{k_y} \cdot \int_{s_0}^{s_1} s^\nu \exp(ak_y s)\cos[k_y(b - sc)]\, ds\, dk_y \tag{25}$$

where a, b, c, and d are constants. When ν is an integer, both integrations can be calculated analytically. However, if ν is not integer, only the spectral integration is performed analytically and the spatial integration is performed numerically. We refer the reader to the Appendix for a full discussion. Circular and elliptic segments yield integrals which are more complicated than (25). However, they can be handled with the same techniques as in the Appendix.

VII. EXAMPLES

A. Illustration of the Use of Parabolic Basis Functions

In this example we demonstrate and discuss the use of a piecewise-parabolic representation for the surface charge density. Along each segment we represent $\rho(s)$ as

$$\rho(s) = s^\mu(A_0 + A_1 s + A_2 s^2), \qquad \mu \geq -0.5. \tag{26}$$

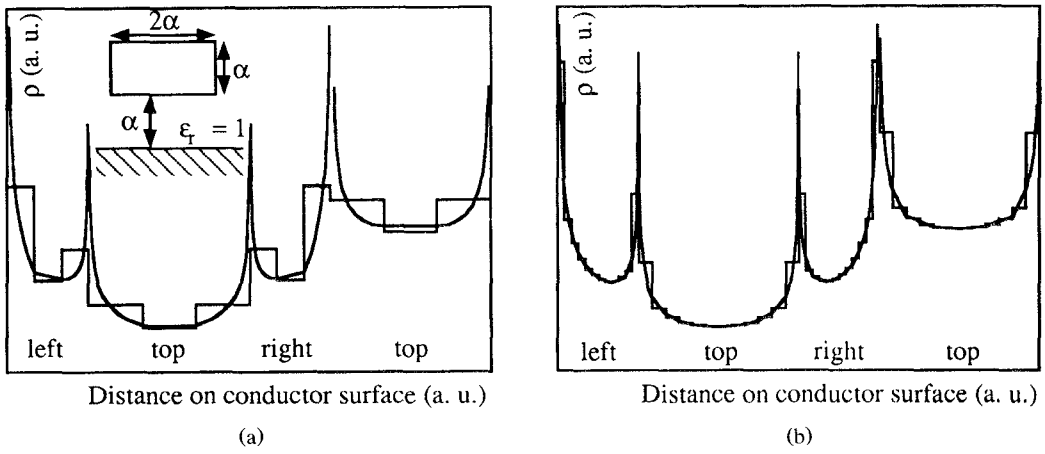

Fig. 3. Piecewise-constant and piecewise-linear representations of the surface charge density on a rectangular conductor with (a) three divisions and (b) 12 divisions on each side.

TABLE III
CAPACITANCE AND RESISTANCE ($r = aR/R_s$) FOR THE RECTANGLE IN FIG. 3

	Three Divisions per Side	12 Divisions per Side
Piecewise-constant representation	$C = 4.4834$ e-11 F/m $r = 0.19747$	$C = 4.5287$ e-11 F/m $r = 0.21085$
Piecewise-linear representation	$C = 4.5382$ e-11 F/m $r = 0.23753$	$C = 4.5377$ e-11 F/m $r = 0.23753$

We have now three unknowns, A_0, A_1 and A_2, in each segment. At the junction of two segments we impose the continuity of $\rho(s)$ and of $d\rho(s)/ds$. There remains one unknown for each segment. Equations for these remaining unknowns are found by means of point matching. The use of recursion relations in integrations of the type (23), (24), and (25) has as a consequence that going from a piecewise-linear representation to a piecewise-parabolic one does not significantly increase CPU time. On the contrary, the use of a parabolic representation allows us to save drastically on the number of segments, as illustrated in the example below. We consider a circular wire with diameter $d = 1$ located at a height, H, above a ground plane in a semi-infinite dielectric with $\epsilon_r = 4$. In Table I the capacitance, C, and the resistance, R, per unit length are given for different numerical approaches when $H = 2$. Losses in the wire are divided by the surface resistance, R_s. We notice that the results for eight piecewise-parabolic segments are as accurate as the results for 24 piecewise-linear segments. In particular, the accuracy of R/R_s is impressive when we use a parabolic representation. In Table II, C and R/R_s are given for $H = 3$, 4, and 5 both for a piecewise-parabolic and for a piecewise-linear representation.

B. Illustration of the Necessity of Having Accurate Surface Charge Density Representations for the Calculation of $\boldsymbol{R}$

In example 3 of [3] the $\boldsymbol{R}$ matrix is given for a combination of four conducting transmission lines. We will show that the results for $\boldsymbol{R}$ presented in [3] have a limited degree of accuracy, taking into account the small number

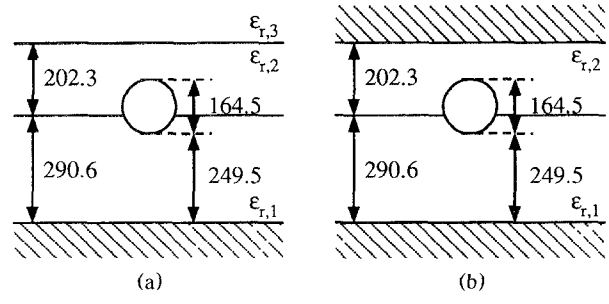

Fig. 4. Typical Multiwire structure in (a) microstrip and (b) stripline configurations.

of segments with piecewise-constant charge density representations used in the numerical approach. To this end we consider a rectangular conductor, with dimensions $\alpha \times 2\alpha$, located in the air at a height α above a ground plane (inset of Fig. 3(a)). Fig. 3(a) shows a surface charge density plot for three segments on each side of the rectangle for piecewise-constant basis functions (blocked line) and piecewise-linear basis functions (continuous line). In Fig. 3(b) we used 12 segments on each side. In Table III the values for C and $r = \alpha R/R_s$ are given. We can see that the use of a small number of piecewise-constant segments is acceptable for the calculation of C. This is because the area under the piecewise-constant charge distribution plot is almost equal to the area under the real charge distribution plot, and C is proportional to this area. R, however, is proportional to the area under the square of the real charge distribution plot (in fact proportional to the square of J_x but we use the equivalent

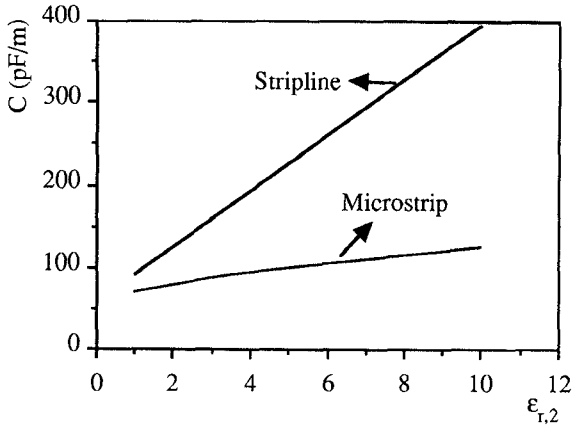

Fig. 5. Capacitance of the wire in Fig. 4(a) and Fig. 4(b) as a function of $\epsilon_{r,2}$.

electrostatic problem terminology). This means that we must have a very accurate charge density representation, especially at singularities, in order to get accurate results for R. We indeed notice in Table III that the values for C are not that far apart, especially when the number of divisions increases. The values for r, however, remain too small when using a piecewise-constant representation, even for an increased number of divisions.

C. Illustration of a Multiwire Bus Structure

The method presented in this paper was developed with the particular aim in mind of also being able to handle new circuit board technologies such as the discrete wiring boards. The next example considers a realistic Multiwire structure with a wire located in a three-layered medium as shown in Fig. 4(a) (microstrip configuration) and Fig. 4(b) (stripline configuration). The dimensions are given in mm and $\epsilon_{r,1} = 4$ and $\epsilon_{r,3} = 1$. In Fig. 5 we show a plot of C as a function of $\epsilon_{r,2}$ for both configurations. We used 24 divisions on each wire. Fig. 6(a) (Fig. 6(b)) shows a plot of the surface charge density on the wire of Fig. 4(a) when $\epsilon_{r,2} = 4.3$ ($\epsilon_{r,2} = 3.7$). The surface charge density becomes zero in Fig. 6(a) and infinite in Fig. 6(b) at the intersection of the layer interface, as predicted by Meixner's condition. In Table IV the $\boldsymbol{C}$, $\boldsymbol{L}$, and $\boldsymbol{R}$ matrices are given for the structure of Fig. 4(a) ($\epsilon_{r,2} = 4.3$) with three wires at the same height numbered from left to right with a center to center separation of 360 mm. The $\boldsymbol{R}$ matrices for losses both in the ground plane and in the wires are given. The results for $\boldsymbol{C}$ and $\boldsymbol{L}$ are given with four to six significant digits. This demonstrates the accuracy of our method because the program was written in single precision with a seven-digit representation.

D. Illustration of the Use of Curved Sides

The last example (Fig. 7) shows the flexibility of our method and in particular the possibility of accurately modeling conductors with a complicated shape. We consider three conductors around a wire above a ground plane. The $\boldsymbol{C}$ matrix is given by

$$\boldsymbol{C} = \begin{pmatrix} 136.00 & -45.33 & -45.33 & -45.33 \\ -45.33 & 128.87 & -36.92 & -36.92 \\ -45.33 & -36.92 & 148.64 & -31.73 \\ -45.33 & -36.92 & -31.73 & 148.64 \end{pmatrix} \text{ pF/m.} \tag{27}$$

Notice that $C_{11} = C_{12} + C_{13} + C_{14}$ to within the numerical accuracy. This means that the central conductor is almost completely shielded from the ground plane.

Appendix

In this Appendix we will go into some detail about the calculation of (25). First we introduce the integral $J(k_c, n, d, b, c)$:

$$J(k_c, n, d, b, c) = \int_{k_c}^{+\infty} \frac{\exp(-k_y d)}{k_y^n} \cos(k_y b + c)\, dk_y. \tag{A1}$$

This integral can be calculated analytically by making use of exponential integrals [10]. The result is

$$\begin{aligned} J = &-\exp(-k_c d) \sum_{i=1}^{n-1} \frac{(-1)^i m^{i-1} (n-i-1)!}{k_c^{n-i} (n-1)!} \\ &\cdot \cos[k_c b + c + (i-1)t] \\ &- \frac{(-1)^n m^{n-1}}{(n-1)!} \Bigg\{ -[\gamma + \ln(k_c m)] \cos[c + (n-1)t] \\ &\cdot + t \sin[c + (n-1)t] \\ &- \sum_{i=1}^{+\infty} \frac{(-1)^i k_c^i m^i}{ii!} \cos[c + (n-1+i)t] \Bigg\} \end{aligned} \tag{A2}$$

with $\gamma = 0.57722\cdots$ being Euler–Mascheroni number, $m = \sqrt{b^2 + d^2}$, and $t = \arctan 2(-b, d)$. The function $-\pi < \arctan 2(x, y) \leq \pi$ is the inverse tangent of x divided by y for four quadrants in the xy plane. When ν is an integer we integrate (25) analytically and get the following result:

$$\begin{aligned} I_n = \sum_{i=1}^{n+1} \Bigg[&\frac{n! s_0^{n+1-i}}{(n+1-i)!} J(k_c, i+1, d - a s_0, b - c s_0, i\tau) \\ &- \frac{n! s_1^{n+1-i}}{(n+1-i)!} J(k_c, i+1, d - a s_1, b - c s_1, i\tau) \Bigg] \end{aligned} \tag{A3}$$

with $\tau = \arctan 2(-c, -a)$. When ν is not an integer the integration over s is calculated numerically and we make a further distinction between $s_0 = 0$ and $s_0 \neq 0$. When s_0 is equal to zero we can place (25), making use of (A2),

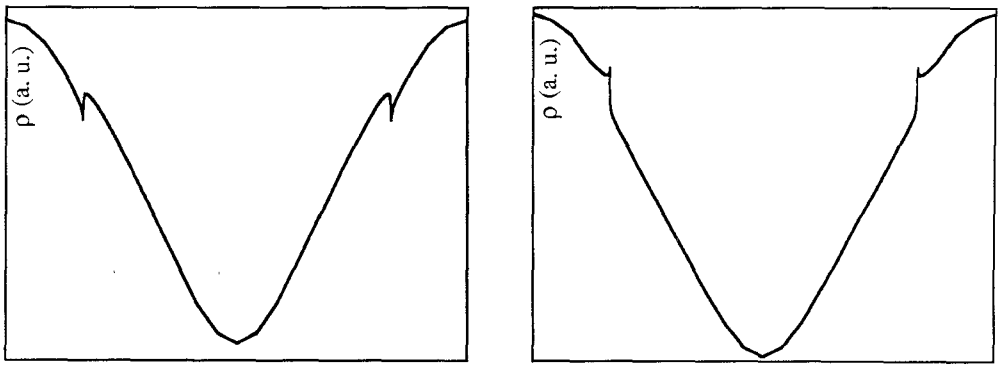

Fig. 6. Surface charge density on the wire of Fig. 4(a) when (a) $\epsilon_{r,2} = 4.3$ and (b) $\epsilon_{r,2} = 3.7$.

TABLE IV
CAPACITANCE, INDUCTANCE, AND RESISTANCE MATRICES FOR A BUS MULTIWIRE STRUCTURE WITH THREE WIRES

Element	C (F/m)	L (H/m)	R/R_s (1/m) Wires	R/R_s (1/m) Ground Plane
11, 33	1.15101 e-10	4.04751 e-7	2.3235 e-3	1.4877 e-3
12, 21, 23, 32	−4.2479 e-11	1.40617 e-7	1.3536 e-4	1.2319 e-3
13, 31	−1.7326 e-12	6.3331 e-8	8.798 e-5	6.0485 e-4
22	1.33432 e-10	3.98183 e-7	2.0851 e-3	1.7456 e-3

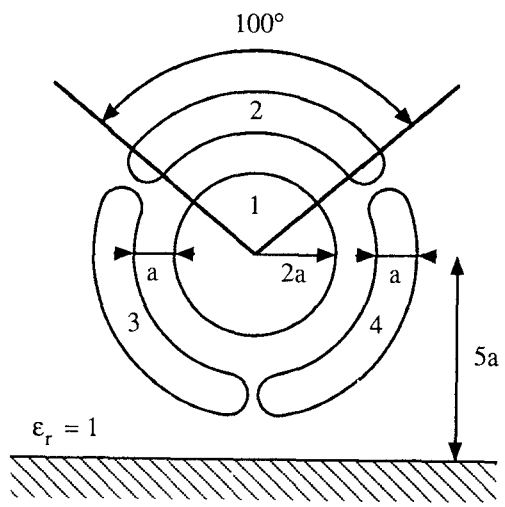

Fig. 7. Curved conductor configuration with three conductors around a wire above a ground plane.

into the following form:

$$I_\nu = s_1^{\nu+1}\left\{ -\frac{\gamma+\ln(k_c)}{\nu+1} - \frac{1}{2}\int_0^1 x^\nu \ln\left[(d-as_1x)^2+(b-cs_1x)^2\right]dx - \sum_{i=1}^{+\infty}\frac{(-1)^i k_c^i}{ii!}\int_0^1 x^\nu\left[\sqrt{(d-as_1x)^2+(b-cs_1x)^2}\right]^i \cdot\cos\left[i\arctan 2(-b+cs_1x, d-as_1x)\right]dx\right\}. \quad \text{(A4)}$$

The remaining integrations are calculated with a Gauss–Jacobi quadrature integration. When $d - as_1 = b - cs_1 = 0$, we cannot use this formula because the first integrand has a logarithmic singularity in $x = 1$. This situation will occur in self-patch calculations. We have to rearrange the integrals. After some calculations we get

$$I_\nu = s_1^{\nu+1}\left\{ -\frac{\gamma+\ln(k_cs_1)+\ln\left(\frac{1}{2}\right)\left[1-\left(\frac{1}{2}\right)^{\nu+1}\right]}{\nu+1} - \frac{1}{2^{\nu+1}}\int_0^1 x^\nu\ln\left(1-\frac{x}{2}\right)dx - \frac{1}{2}\int_0^1\ln(x)\left(1-\frac{x}{2}\right)^\nu dx - \sum_{i=1}^{+\infty}\frac{(-1)^i(k_cs_1)^i}{ii!} \cdot\cos\left[i\arctan 2(-c,a)\right]\sum_{j=0}^{i}\frac{C_i^j(-1)^j}{\nu+j+1}\right\}. \quad \text{(A5)}$$

The first integral is calculated with a Gauss–Jacobi quadrature. The second is calculated with a special Gauss quadrature for logarithmic singularities. When s_0 is not equal to zero we can put (25) in a form similar to (A4), except that now we use Gauss quadratures instead of Gauss–Jacobi quadratures. In the case of self-patch calculations we get a formula analogous to (A5) with integrands which again have logarithmic singularities.

REFERENCES

[1] W. Delbare and D. De Zutter, "Space-domain Green's function approach to the capacitance calculation of multiconductor lines in multilayered dielectrics with improved surface charge modelling," *IEEE Trans. Microwave Theory Tech.*, vol. 37, pp. 1562–1568, Oct. 1989.

[2] C. Wei, R. F. Harrington, J. R. Mautz, and T. K. Sarkar, "Multiconductor transmission lines in multilayered dielectric media," *IEEE Trans. Microwave theory Tech.*, vol. MTT-32, p. 439, Apr. 1984.

[3] R. F. Harrington and C. Wei, "Losses on multiconductor transmission lines in multilayered dielectric media," *IEEE Trans. Microwave Theory Tech.*, vol. MTT-32, pp. 705–710, July 1984.

[4] N. Faché and D. De Zutter, "Rigorous full-wave space-domain solution for dispersive microstrip lines," *IEEE Trans. Microwave Theory Tech.*, vol. 36, pp. 731–737, Apr. 1988.

[5] N. Faché and D. De Zutter, "Full-wave analysis of a perfectly conducting wire transmission line in a double-layered conductor-backed medium," *IEEE Trans. Microwave Theory Tech.*, vol. 37, pp. 512–516, Mar. 1989.

[6] N. Faché, J. Van Hese, and D. De Zutter, "Generalised space domain Green's dyadic for multilayered media with special application to microwave interconnections," *J. Electromagn. Waves and Appl.*, vol. 3, no. 7, pp. 651–669, 1989.

[7] K. A. Michalski and D. Zheng, "Rigorous analysis of open microstrip lines of arbitrary cross section in bound and leaky regimes," *IEEE Trans. Microwave Theory Tech.*, vol. 37, pp. 2005–2010, Dec. 1989.

[8] N. Faché, "High frequency analysis of two dimensional electrical interconnections," Ph.D. thesis, Laboratory of Electromagnetism and Acoustics, Ghent Univ., Ghent, Belgium, Dec. 1989.

[9] J. Meixner, "The behaviour of electromagnetic fields at edges," *IEEE Trans. Antennas Propagat.*, vol. AP-20, pp. 442–446, July 1972.

[10] M. Abramowitz and I. A. Stegun, Eds., *Handbook of Mathematical Functions* (Applied Mathematics Series–55). Washington, DC: National Bureau of Standards, Dec. 1965, p. 229.

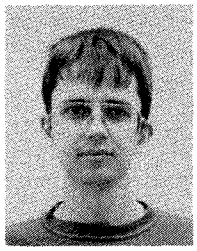

Frank Olyslager (S'90) was born in Wilrijk, Belgium, on November 24, 1966. He received a degree in electrical engineering from the University of Ghent in July 1989. At present he is working toward the Ph.D. degree in electrical engineering at the University of Ghent as a Research Assistant of the National Fund for Scientific Research of Belgium. His research concerns the electromagnetic modeling of high-frequency interconnections.

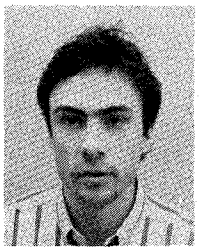

Niels Faché was born in Ghent, Belgium, on July 4, 1964. He received a degree in electrical engineering from the University of Ghent in July 1986. In December 1989 he obtained the Ph.D. degree from the Laboratory of Electromagnetism and Acoustics (LEA) at the University of Ghent. His research dealt with the full-wave analysis and circuit modeling of two-dimensional electrical interconnections embedded in multilayered media.

In 1990 he worked as a consultant from LEA to the Network Measurements Division (Santa Rosa, CA) of the Hewlett-Packard Company (HP). While at HP, he worked on the improvement of linear models in the Microwave Design System (MDS) and the implementation of new linear models. Currently, he is back at LEA, where his research now focuses on electromagnetic field solvers and their use in circuit simulators.

Daniël De Zutter was born in Eeklo, Belgium, on November 8, 1953. He received a degree in electrical engineering from the University of Ghent in July 1976. From September 1976 to September 1984 he was a research and teaching assistant in the Laboratory of Electromagnetism and Acoustics (LEA) at the same university. In October 1981 he obtained the Ph.D. degree there and in the spring of 1984 he completed a thesis leading to a degree equivalent to the French Aggrégation or the German Habilitation.

Most of his earlier scientific work dealt with the electrodynamics of moving media, with emphasis on the Doppler effect and the forces involved in the interaction of fields with moving media. At present he works at the LEA as a Research Associate of the National Fund for Scientific Research of Belgium. His research now focuses on all aspects of circuit and electromagnetic modeling of high-frequency and high-speed interconnections.